Available online at www.sciencedirect.com
SCIENCE DIRECT®
Microelectronic Engineering 73–74 (2004) 604–609
MICROELECTRONIC ENGINEERING
www.elsevier.com/locate/mee

The effect of encapsulation on the morphology and chemical composition of InAs/GaAs quantum dots grown by molecular beam epitaxy

D. Zhi [a,*], M. Wei [a], R.E. Dunin-Borkowski [a], P.A. Midgley [a], D.W. Pashley [b], T.S. Jones [c], B.A. Joyce [d], P.F. Fewster [e], P.J. Goodhew [f]

[a] *Department of Materials Science and Metallurgy, University of Cambridge, Pembroke Street, Cambridge CB2 3QZ, UK*
[b] *Department of Materials, Imperial College, London SW7 2AY, UK*
[c] *Department of Chemistry, Imperial College, London SW7 2AY, UK*
[d] *Department of Physics, Imperial College, London SW7 2AY, UK*
[e] *PANalytical Research Centre, Redhill RH1 5HA, UK*
[f] *Department of Engineering, University of Liverpool, Liverpool L69 3GH, UK*

Available online 14 March 2004

Abstract

In order to fabricate an effective device structure based on InAs quantum dots (QDs), the QD layers must be encapsulated within a matrix that has a wider band gap. This encapsulation is usually achieved by the overgrowth of GaAs. Coherent strained InAs/GaAs islands, which were previously formed on the (0 0 1) GaAs substrate surface, can then be buried in the semiconductor matrix to form QDs. The capping process has a significant effect on the structure and properties of QDs. In the present study, a range of transmission electron microscopy (TEM) techniques is used to characterise both the microstructure and the chemistry of the QDs with different capping layer thickness. High-resolution in-plane X-ray scattering is also applied to characterise the QD structures. Uncapped InAs/GaAs QDs are found to be multi-faceted. The formation of {1 1 3} facets and {1 1 1} growth steps is clearly visible along the [1 $\bar{1}$ 0] zone axis in high-resolution TEM images. Following the capping process, the QD density is observed to decrease, presumably due to lateral spreading and coalescence. As a result of mass transport and interdiffusion during growth of the first few monolayers of the GaAs capping layers, the in content in the QDs is reduced, with the final In content in a fully buried QD determined to be 65–67%.

Keywords: Indium arsenide; Quantum dots; Encapsulation; Transmission electron microscopy

1. Introduction

The optoelectronic properties of quantum dot (QD) devices are influenced by the size, shape, arrangement, crystal morphology, and chemical

* Corresponding author. Tel.: +44-0-1223-334564; fax: +44-0-1223-334567.
E-mail address: dz215@cam.ac.uk (D. Zhi).

0167-9317/$ - see front matter © 2004 Elsevier B.V. All rights reserved.
doi:10.1016/j.mee.2004.02.093

composition of the QDs [1]. Among the different QD systems, the formation of self-assembled InAs QDs on GaAs (0 0 1) substrates, in particular, continues to be an intensively studied subject. Many structural studies have shown that the properties of the QDs depend on the growth conditions, such as growth temperature, beam flux rates, growth interruptions, and InAs coverage [2,3]. For InAs QDs to be used in an optoelectronic device, they must be embedded in a confining layer, typically GaAs. During the encapsulation process, differences in lattice parameters between QD and capping layer result in strain, which in turn affects the electronic properties of the device [4]. The capping process also affects the shape and the composition of the QD [5–7]. An improved understanding of the processes involved in QD encapsulation is therefore beneficial for refining the growth of optically useful QD systems. In the present study, InAs/GaAs (0 0 1) QD structures with different GaAs capping layer thicknesses were fabricated by molecular beam epitaxy (MBE). A range of transmission electron microscopy (TEM) techniques, including diffraction contrast, high-resolution lattice imaging, and analytical electron microscopy, were used to characterise both the microstructure and the chemistry of the QDs close to the atomic scale. High-resolution X-ray scattering was also applied to characterise the capped InAs QD structures. The collective structural information obtained by X-ray scattering method was compared with more localized information obtained using TEM-based techniques.

2. Experimental

Growth of InAs/GaAs QDs was carried out in a purpose-built MBE system [8]. The QD samples were grown by depositing 2 monolayers (ML) InAs with an In flux of 1.08×10^{14} atoms $cm^{-2} s^{-1}$, which corresponds to a deposition rate of 0.2 $ML s^{-1}$, at a growth temperature of 510 °C. One sample was kept uncapped as a reference and the others were subsequently overgrown at the same growth temperature with a GaAs layer of different thickness, using a Ga flux of 6.26 atoms $cm^{-2} s^{-1}$ (1.0 $ML s^{-1}$). The as-grown QD samples were initially examined using an atomic force microscope (AFM) (Burleigh Metris 2000) operating in non-contact mode.

TEM plan-view and cross-section specimens were prepared using conventional sample preparation techniques, involving mechanical thinning followed by ion-milling using Ar^+ at 3–5 keV. Thinned specimens were examined using a JEOL 2010 TEM and the compositional analysis was performed using a field emission gun STEM (VG HB601-UX).

High-resolution reciprocal space maps were recorded using a commercially available Philips materials research diffractometer with in-plane X-ray scattering geometry. With this high-resolution configuration, the strain sensitivity is excellent and the diffuse scattering that arises from the strain modulation can be compared with simulations in order to derive the size, shape and composition of the QDs. In our scattering data analysis, the approach based on the analysing the influences associated with the lateral inhomogeneities, i.e., the strain fields of QDs, which was used to simulate the in-plane scattering results [9].

3. Results and discussion

3.1. Uncapped InAs QDs

An ex situ AFM image of an uncapped QD sample is shown in Fig. 1(a). The QD density is $\sim 1.3 \times 10^{10}$ cm^{-2} and the lateral dimension of the QDs along [1 $\bar{1}$ 0] is ~20–30 nm. The density and the dimensions have been confirmed by a plan-view TEM bright field (BF) image taken along the [0 0 1] zone axis, as shown in Fig. 1(b). The image shows pronounced strain contrast effect and a 90° cross-shaped strain contrast with the two cross-directions along [0 1 0] and [1 0 0] respectively. Fig. 1(c) shows a high-resolution cross-sectional TEM image of an uncapped InAs QD, which was taken along [1 $\bar{1}$ 0]. The image appears to show that the QD is bounded by (1 1 3) and ($\bar{1}$ $\bar{1}$ 3) facets, although strictly it is not possible to distinguish between edges and faces. Similar (1 1 3) faceted planes have previously been observed for InAs islands on GaAs (0 0 1) by

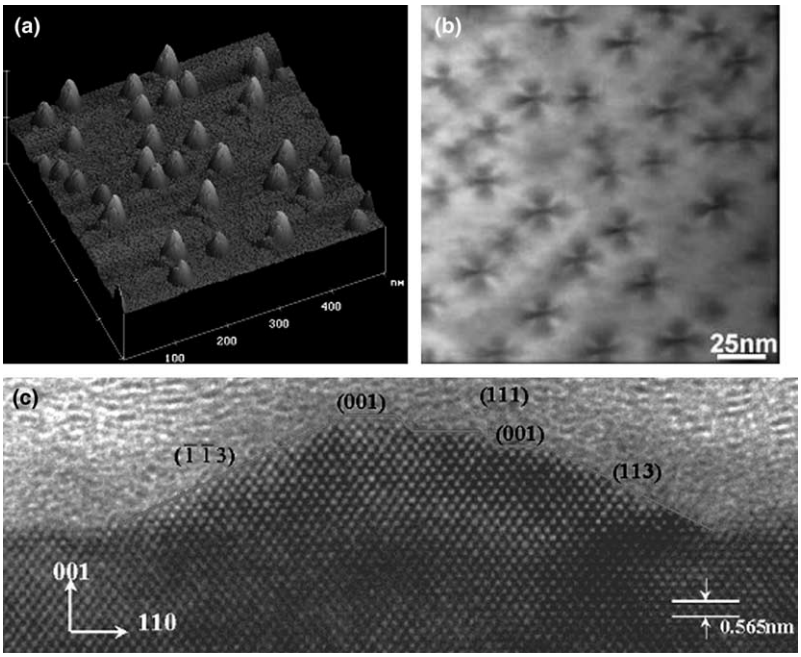

Fig. 1. (a) AFM image of uncapped QDs, (b) [0 0 1] zone plan-view BF TEM image of unburied QDs, and (c) [1 $\bar{1}$ 0] zone HRTEM image of uncapped QDs.

scanning tunnelling microscopy (STM) [10]. However, the appearance of chevron features on reflection high-energy electron diffraction (RHEED) patterns [5] indicates that the bounding surfaces of the QD are curved. Since the cross-sectional HRTEM image effectively presents a profile of the QD along [1 $\bar{1}$ 0], it is not inconsistent with the existence of a curved boundary. The formation of {1 1 3} facets and {1 1 1} growth steps, which are visible in the HRTEM image, results in curved boundaries on the QDs.

3.2. Initial stage of encapsulation

Following the capping process, the QD density was observed to decrease, presumably due to lateral spreading and coalescence. Typical cross-sectional HRTEM image in Fig. 2(a) shows the obvious morphological changes of QD after only 0.5 nm of GaAs overgrowth (~2 ML). It can be found from the TEM image that at the initial stage of GaAs overgrowth, the QD height tends to be slightly shorter and the lateral dimension longer. It is believed that the GaAs is deposited initially at the edge of the QD/substrate interface. When two QD islands are formed next to each other, the GaAs overgrowth promotes the coalescence of the two adjacent QDs, as shown in Fig. 2(b). This phenomenon was observed particularly from the InAs/GaAs QD samples grown using a typical MBE growth rate of 0.1–0.6 ML s^{-1} for the pure InAs deposition for the QD layer.

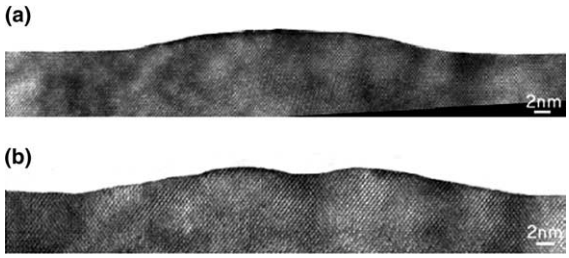

Fig. 2. [1 1 0] Zone cross-sectional HRTEM images of, (a) an isolated QD, and (b) two neighbouring QDs after 5Å GaAs capping.

Further deposition of GaAs leads to more dramatic changes in surface morphology. Fig. 3 shows a cross-sectional HRTEM image obtained from a 1.5 nm capped QD sample. The image

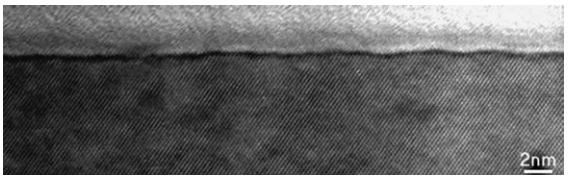

Fig. 3. Cross-sectional HRTEM image of QD after 15Å GaAs capping.

shows that the capped QD is apparently coherent with the GaAs matrix, however it now becomes difficult to distinguish the QD shape. Similar results by RHEED and STM studies were also reported on the capped InAs QD sample using the same conventional growth rate [11].

3.3. Fully capped InAs QDs

Cross-sectional TEM images revealed the presence of a continuous InAs wetting layer between the GaAs substrate and the GaAs capping layer, as shown in Fig. 4(a). The image shows the buried QD is formed on a continuous wetting layer. The existence of the wetting layer can be illustrated by the intensity profile in Fig. 4(b). The wetting layer thickness can be estimated as 1.5 nm by fitting the wetting layer peak in the intensity profile. To confirm this QD-on-wetting layer structure, a cross-sectional high-angle annular dark field (HAADF) STEM image was taken parallel to the $\langle 1\,1\,0\rangle$ direction, as shown in Fig. 4(c). The image shows atomic number Z contrast of the QDs, the wetting layer and surrounding GaAs matrix and demonstrates that the QDs are formed on the wetting layer. A series of EDX line scans across the QD was also recorded along the interface direction. The widths (FWHM) of these indium peaks are plotted as a function of the distance from the QD centre in Fig. 4(d). This line profile can be used to determine the actual lateral size of the buried QD (~45 nm in this case).

3.4. Compositional evolution during encapsulation

In Fig. 5(a), we show a STEM image obtained from a fully capped QD sample, in which three

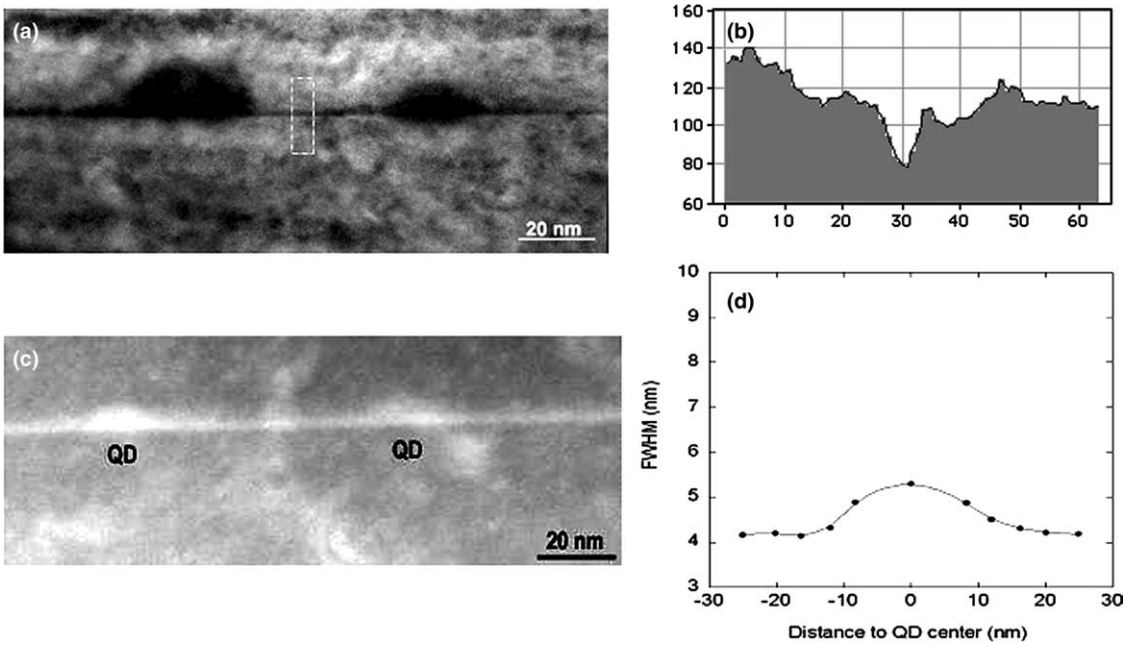

Fig. 4. (a) TEM bright field image of InAs QD buried in GaAs matrix, (b) intensity profile from the marked region showing the wetting layer in the image (a), (c) HAADF image of small coherent InAs QD in GaAs matrix, and (d) EDX peak width (FWHM) at different lateral position of a buried QD.

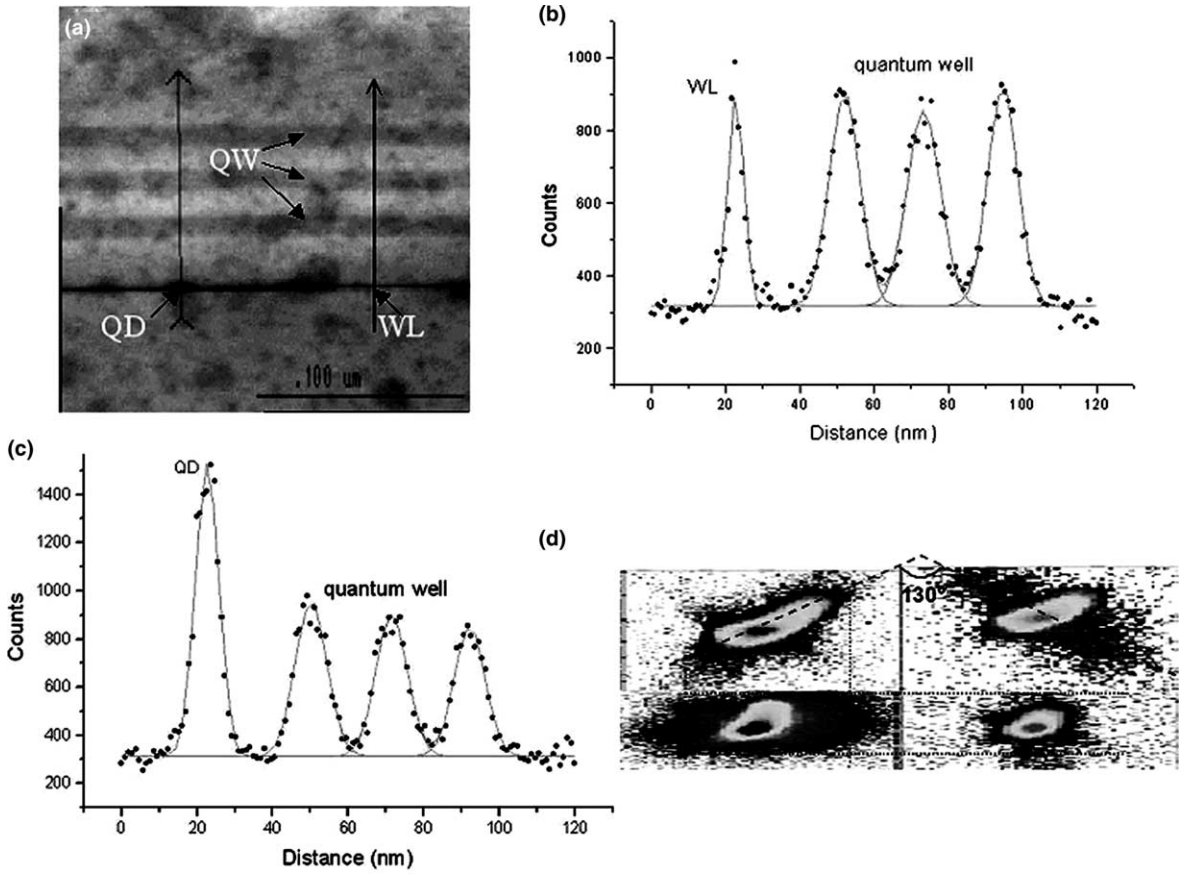

Fig. 5. (a) STEM image from a QD sample containing three $In_{0.12}Ga_{0.88}As$ QWs, (b) and (c) show EDX line-scan profiles through wetting layer and QD, respectively, (d) 400, 040, 220 and −220 experimental reciprocal space maps from in-plane X-ray scattering.

quantum wells (QWs) with a composition of $In_{0.12}Ga_{0.88}As$ were grown after the encapsulation of the QD layer. Fig. 5(b) and (c) show corresponding EDX line-scans (In profiles) taken through the QWs and the QD (b), and the QWs and wetting layer (c), respectively. Both line-scans were fitted with Gaussian function and the background was subtracted. The results show that there is virtually no peak overlap. For the case of a pyramid QD, the In content of the QDs was calculated to be ~66% [7], while the In content in the wetting layer was calculated to be ~12%. We also found that the detailed QD shapes had only a small effect on the measured. In composition value through the apex and central region of the QD, although it became increasingly important towards the peripheries of the dots. For the other QD shapes we have considered, the calculated indium compositions from the same line-scan were: truncated pyramid 63%, hemispherical cap 66% and cone 71%. Using a similar approach, we found that the measured In contents of about 90% in uncapped QDs and about 70% in partly capped QDs, are higher than the value of 65–67% in fully buried QDs. This decrease of the In content of QDs during encapsulation can be attributed to out-diffusion during the encapsulation process.

Fig. 5(d) shows in-plane X-ray scattering experimental results obtained from the same sample that was examined in Fig. 5(a). The diffuse in-plane X-ray scattering associated with the dots was weak but observable, giving characteristic, almost anti-symmetric patterns between the 400 and 040

reflections, as well as distinct differences between the 220 and −220 reflections. Using the method described in [9], the best fit, comparing with the STEM analysis, is $(25 \pm 3$ nm$) \times (25$–40 nm$) \times (5 \pm 0.5$ nm) for the shape and $48\% \rightarrow 55\%$ for the In composition (assuming the dot to be 25nm and circular in projection), although this could be reduced to as much as $30\% \rightarrow 35\%$ if the dot investigated is asymmetric in shape with dimension of 25×40 nm. The difference in results between STEM and X-ray scattering is mainly due to the different sampling area of the two methods. The X-ray method measures from the whole wafer and give an average result for all the dots, while STEM method measures only the central area of one single dot. Apparently, the composition near the dot edge will be significantly lower than the central value, which will give a lower composition value for the average of whole dot.

4. Conclusions

Changes in the structure and composition of InAs/GaAs QDs have been investigated. The uncapped InAs/GaAs QDs are multi-facetted and the apparent $\{1\,1\,3\}$ facets observed parallel to the $[1\,\bar{1}\,0]$ zone axis in HRTEM images are consistent with curved boundaries to the QDs. Following the capping process, the nominal QD density is found to decrease as a result of lateral spreading and coalescence. The In content of the QDs is also reduced as a result of the GaAs encapsulation, with the final In content in a fully buried QD, grown at a rate of 0.01 ML s^{-1} and a temperature of 510 °C, determined to be 65–67%. The morphological and compositional changes observed for the QDs occurred within the first 2 MLs of GaAs capping, indicating the extent of mass transport in the early stages of the process.

References

[1] D. Bimberg, M. Grundmann, N.N. Ledentsov, MRS Bull. 2 (1998) 31.
[2] P.B. Joyce, T.J. Krzyzewski, G.R. Bell, T.S. Jones, S. Malik, D. Childs, R. Murray, Phys. Rev. B 62 (2000) 10891.
[3] I. Mukhametzhanov, Z. Wei, R. Heitz, A. Madhukar, Appl. Phys. Lett. 75 (1999) 85.
[4] G.D. Lian, J. Yuan, L.M. Brown, G.H. Kim, D.A. Ritchie, Appl. Phys. Lett. 73 (1998) 49.
[5] D.W. Pashley, J.H. Neave, B.A. Joyce, Surf. Sci. 476 (2001) 35.
[6] T. Walther, A.G. Cullis, D.J. Norris, M. Hopkinson, Phys. Rev. Lett. 86 (2001) 2381.
[7] D. Zhi, H. Davock, R. Murray, C. Roberts, T.S. Jones, D.W. Pashley, P.J. Goodhew, B.A. Joyce, J. Appl. Phys. 89 (2001) 2079.
[8] B.A. Joyce, T.S. Jones, J.G. Belk, J. Vac. Sci. Technol. B 16 (1998) 2372.
[9] P.F. Fewster, V. Holy, D. Zhi, J. Phys. D: Appl. Phys. 36 (2003) A217.
[10] Y. Hasegawa, H. Kiyama, Q.K. Xue, T. Sakurai, Appl. Phys. Lett. 72 (1998) 2265.
[11] P.B. Joyce, T.J. Krzyzewski, G.R. Bell, T.S. Jones, Appl. Phys. Lett. 79 (2001) 3615.